IJETIR

ISSN (Online) 2583-0554

International Journal of Emerging Technologies and Innovative Research (IJETIR)

Volume 3, Issue 1, February 2023

Impact Factor: 5.731

Synthesis and characherization of of $ZnFe_2O_4$ nanoparticles via Sol-Gel Auto-Combustion: Structural, Magnetic, and Electrical Characterization

Atul P. Keche*[a]

[a]Department of Physics

R. B. Attal Arts, Science & Commerce College, Georai, Beed, India

Corresponding author: meetatulkeche@gmail.com

Abstract: *$ZnFe_2O_4$ magnetic nanoparticles were successfully synthesized via the sol–gel auto-combustion route using citric acid ($C_6H_8O_7$) as the fuel. X-ray diffraction (XRD) analysis confirmed the formation of a cubic spinel structure with Fd3m (Oh^7) space-group symmetry and a lattice parameter of 8.4 ± 0.05 Å. The average crystallite size, estimated from peak broadening using the Debye–Scherrer equation, was approximately 36 nm. Fourier-transform infrared (FT-IR) spectroscopy revealed two characteristic metal–oxygen vibrational bands at ~550 cm^{-1} and ~400 cm^{-1}, corresponding to octahedral (O-M Td)and tetrahedral (O-M Td) sites, respectively, thereby confirming the spinel structure. Magnetic measurements yielded the saturation magnetization (Ms), remanent magnetization (Mr) and magnetic moment (n_B) Furthermore, DC electrical resistivity studies following Arrhenius behavior established the semiconducting nature of the synthesized $ZnFe_2O_4$ nanoparticles*

Keywords*:* Nanoparticles; Solgel; *IR* spectroscopy; magnetic property; *DC*-Electrical property

I. INTRODUCTION

Spinel zinc ferrite nanoparticles ($ZnFe_2O_4$) represent an important class of magnetic nanomaterials that combine a unique set of physical, chemical, and functional properties, rendering them promising for a broad spectrum of advanced technological applications [2]. Their fundamental functionality originates from intrinsic ferrimagnetism, which arises due to the antiparallel alignment of magnetic moments within the spinel crystal lattice, leading to the emergence of a net magnetic moment [3]. When coupled with nanoscale dimensions, this magnetic behavior results in high responsiveness to externally applied magnetic fields, allowing precise manipulation and control. Consequently, $ZnFe_2O_4$ nanoparticles have attracted significant interest for targeted biomedical applications, including magnetic drug delivery systems, hyperthermia-based cancer therapy, and contrast enhancement in magnetic resonance imaging (MRI) [4].

In addition to biomedical uses, $ZnFe_2O_4$ nanoparticles exhibit outstanding characteristics that enable their application across diverse technological domains. These include soft magnetic components for high-frequency, low-loss devices, gas-sensing materials, semiconductor photocatalysts, and energy-related systems such as magnetocaloric pumps [5]. Recent investigations have demonstrated the high sensitivity of $ZnFe_2O_4$ nanoparticles toward various gases, including methane (CH_4), hydrogen sulfide (H_2S), liquefied petroleum gas (LPG), and ethanol (C_2H_5OH), highlighting their effectiveness in gas-sensing technologies [5]. Such performance emphasizes their importance in environmental monitoring and industrial gas detection, underscoring their versatility in both scientific and practical applications[7].

$ZnFe_2O_4$ nanoparticles also exhibit excellent chemical and thermal stability, maintaining structural and functional integrity under harsh chemical environments, elevated temperatures, and corrosive conditions. This inherent robustness makes them well suited for demanding applications such as environmental remediation, where they function as efficient catalysts for pollutant degradation, as well as energy storage systems, in which their stability contributes to enhanced

IJETIR
ISSN (Online) 2583-0554
International Journal of Emerging Technologies and Innovative Research (IJETIR)
Volume 3, Issue 1, February 2023
Impact Factor: 5.731

electrochemical performance [6]. Furthermore, the nanoscale size of these particles results in a high surface-to-volume ratio, significantly enhancing surface reactivity and catalytic efficiency.

Beyond their magnetic and catalytic behavior, $ZnFe_2O_4$ nanoparticles possess notable optical properties, including strong absorption in the visible and near-infrared regions of the electromagnetic spectrum. This feature makes them attractive candidates for optoelectronic applications such as photodetectors and solar energy conversion devices. The synergistic combination of magnetic, chemical, and optical characteristics establishes $ZnFe_2O_4$ nanoparticles as multifunctional materials with considerable potential in data storage, catalysis [7], environmental remediation[8], energy conversion technologies, and biomedical fields [9].

Spinel ferrites, generally expressed by the formula $MeFe_2O_4$ (where Me denotes divalent metal cations such as Fe^{2+}, Co^{2+}, Ni^{2+}, Cu^{2+}, Mg^{2+}, or Zn^{2+}), have garnered extensive research interest owing to their favorable electromagnetic properties, chemical stability, mechanical robustness, and tunable magnetic behavior[10]. Among them, zinc ferrite nanoparticles have been widely investigated due to their high electromagnetic performance, low coercivity, moderate saturation magnetization, and superior stability. In the present study, $ZnFe_2O_4$ nanoparticles were synthesized using the sol–gel auto-combustion technique, a method recognized for its simplicity, cost-effectiveness, and ability to produce nanoparticles with excellent chemical homogeneity and structural uniformity. Compared with other synthesis routes, the sol–gel auto-combustion method offers enhanced molecular-level mixing of precursors, enabling precise control over particle size, morphology, and compositional uniformity [11].

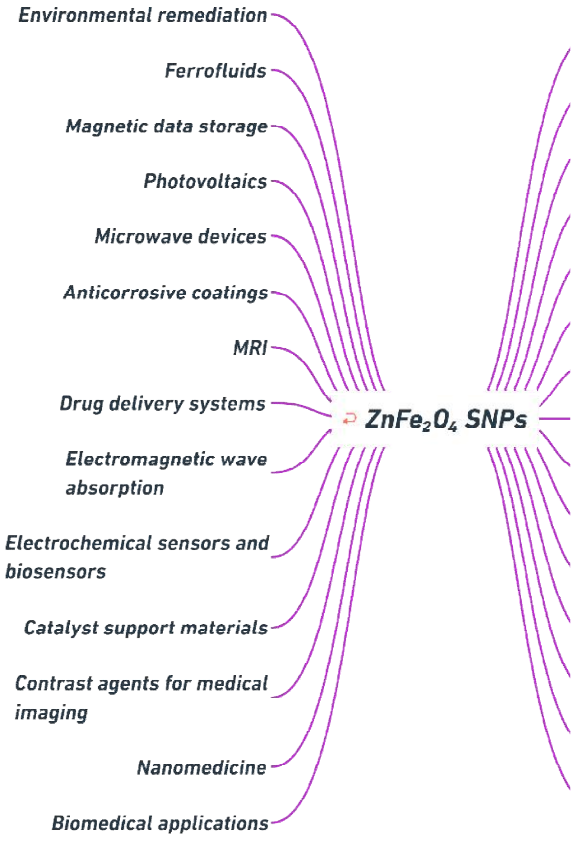

Figure 1. Various applications of $ZnFe_2O_4$ Nanoparticles

This method guarantees the creation of $ZnFe_2O_4$Nanoparticles with high purity and structural integrity. This extensive study investigates how the sol-gel auto-combustion technique affects the structural and magnetic properties of $ZnFe_2O_4$Nanoparticles. The capacity to manage and enhance the physical characteristics of $ZnFe_2O_4$Nanoparticles via sol-gel synthesis and subsequent characterization techniques holds significant promise for developing advanced

IJETIR
ISSN (Online) 2583-0554
International Journal of Emerging Technologies and Innovative Research (IJETIR)
Volume 3, Issue 1, February 2023
Impact Factor: 5.731

materials with tailored functionalities. Such innovations could be crucial in emerging technologies, including magnetic data storage, catalysis, gas sensing, and biomedical applications. The advancements in the synthesis and characterization of spinel ferrites like $ZnFe_2O_4$ are anticipated to expand their use in novel industrial and technological solutions.

II. EXPERIMENTAL

2.1 Materials

AR-grade (99.9% purity) chemicals procured from Fisher Scientific Pvt. Ltd. were used as received to ensure high reproducibility and reliability of the synthesis. The reagents included ferrous nitrate ($Fe(NO_3)_3 \cdot 9H_2O$) as the iron source, zinc nitrate ($Zn(NO_3)_2 \cdot 6H_2O$) as the zinc source, citric acid ($C_6H_8O_7$) as a chelating agent for homogeneous metal–citrate complex formation, ammonia solution for pH adjustment and controlled precipitation, and deionized water as the solvent to minimize impurities. The use of high-purity reagents reduced contamination and undesirable side reactions, ensuring consistent and accurate experimental outcomes.

2.2 Synthesis of $ZnFe_2O_4$ Nanoparticles

$ZnFe_2O_4$ nanoparticles were synthesized via the sol–gel auto-combustion method using stoichiometric amounts of AR-grade ferric nitrate ($Fe(NO_3)_3 \cdot 9H_2O$) and zinc nitrate ($Zn(NO_3)_2$) with 99.9% purity. The metal nitrates were dissolved in deionized water and complexed with citric acid ($C_6H_8O_7$) at a 1:3 molar ratio to form a homogeneous precursor. The solution pH was adjusted to 7 using ammonia solution to optimize gel formation and combustion behavior. The mixture was heated at 70–80 °C under continuous stirring until gelation, followed by spontaneous auto-combustion, yielding a fluffy pre-sintered $ZnFe_2O_4$ powder through an exothermic redox reaction between nitrates and citric acid.

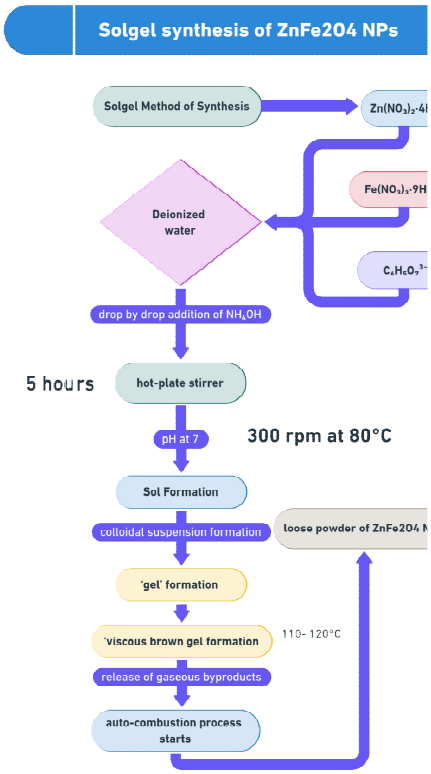

Figure 1 schematic overview of sol-gel auto-combustion synthesis process of $ZnFe_2O_4$ Nanoparticles.

The resulting powder was slowly cooled to room temperature, ground to ensure uniformity, and pressed into disc-shaped pellets (10 mm diameter, 3 mm thickness) under a pressure of 5 tons cm^{-2} for 5 min. This environmentally

benign synthesis route demonstrates the efficiency and scalability of the sol–gel auto-combustion method for producing phase-pure $ZnFe_2O_4$ nanoparticles.

2.3 Characterizations of $ZnFe_2O_4$Nanoparticles

The synthesized $ZnFe_2O_4$ nanoparticles were characterized using complementary analytical techniques. X-ray diffraction (XRD), performed at room temperature using a Bruker D-8 diffractometer with Cu–Kα radiation, confirmed the formation of the spinel phase and the absence of secondary phases. Fourier-transform infrared (FT-IR) spectroscopy was employed to analyze metal–oxygen bonding and residual functional groups. Magnetic properties, including coercivity, remanence, and saturation magnetization, were evaluated using a pulse-field hysteresis loop tracer. Electrical behavior was investigated through DC resistivity measurements on pelletized samples using the two-probe method. Collectively, these techniques provided a comprehensive assessment of the structural, chemical, magnetic, and electrical properties of the $ZnFe_2O_4$ nanoparticles, validating the effectiveness of the sol–gel auto-combustion synthesis route and supporting their suitability for advanced technological applications.

III. RESULTS AND DISCUSSION

3.1 X-ray diffractionof $ZnFe_2O_4$Nanoparticles

X-ray diffraction (XRD) patterns of $ZnFe_2O_4$Nanoparticles were acquired using a Model X'PertPRO MPD PANalytical system at room temperature, both before and after exposure to 100 kGy of gamma irradiation. Data was collected over a 2θ range of 20° to 80° using $Cu-K\alpha$ radiation ($\lambda = 1.5405$ Å) with a step size of 0.02° and a 1 −second count time per step, resulting in a total data acquisition time of 3 hours. The observed Bragg reflections were compared to the $JCPDS$ card number $22-1012$[12] to confirm the presence of a single-phase $ZnFe_2O_4$ with a face-centered cubic spinel structure. XRD analysis is crucial for differentiating between size-induced and strain-induced broadening of diffraction peaks, which can be effectively analyzed by fitting Lorentzian and Gaussian profiles to characteristic peaks such as (220) and (440). Figure 2 illustrates the XRD pattern of $ZnFe_2O_4$ magnetic Nanoparticles synthesized via the sol-gel auto-combustion method at room temperature, covering a (2θ) range of 20°– 80°.The X-ray diffraction (XRD) pattern confirms the successful synthesis of crystalline zinc ferrite ($ZnFe_2O_4$) Nanoparticles with a cubic spinel structure. Sharp and distinct diffraction peaks, indexed by Miller indices such as $(311), (220), (400), (422), (511), (440), and\ (622)$,[13] are observed, indicating a well-defined crystal structure. The most intense peak, corresponding to the (311) plane, is characteristic of spinel ferrites. The absence of any secondary peaks in the XRD pattern confirms the phase purity of the synthesized sample, indicating the absence of detectable impurities. These results collectively demonstrate the successful formation of a single-phase, highly crystalline zinc ferrite [16]. The formula for lattice constant was;

$$a = d_{hkl}\sqrt{h^2 + k^2 + l^2} \quad (1)$$

where d is the interplanar spacing, a is the lattice constant, and hkl are the Miller indices of each plane in the family. The lattice parameter value for $ZnFe_2O_4$Nanoparticles was determined using the Debye-Scherrer formula [20, 21];

$$D = \frac{k\lambda}{\beta \cos\theta} \quad (2)$$

Here, k is a constant with a value of $0.89, \lambda$ is the wavelength of the X-ray source (1.5405 Å), β represents the full width at half maximum ($FWHM$), and θ is the glancing angle.

IJETIR
ISSN (Online) 2583-0554
International Journal of Emerging Technologies and Innovative Research (IJETIR)
Volume 3, Issue 1, February 2023
Impact Factor: 5.731

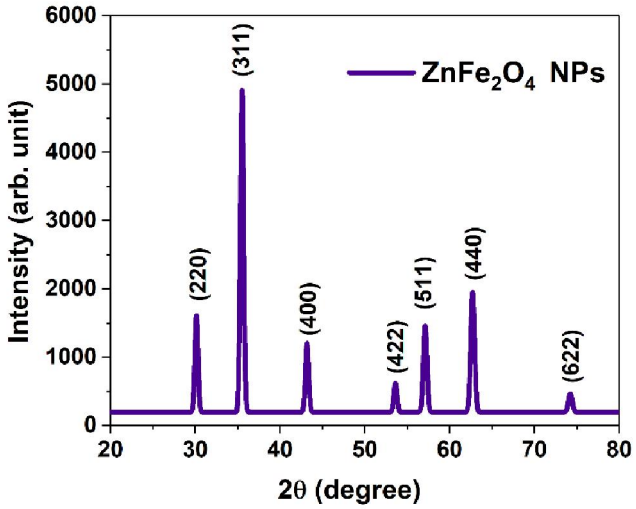

Figure 2 X-ray diffraction (XRD) pattern of $ZnFe_2O_4$ Nanoparticles

This confirms the formation of a well-structured cubic spinel crystal with minimal distortions. These results indicate that the Nanoparticles exhibit high crystalline quality, aligning with the expected properties of ferrite materials. The observed decrease in d-spacing with increasing Bragg's angle follows standard crystallographic behavior, validating the accuracy of the measurements and the integrity of the synthesized material. Based on this relationship, the X-ray density (dx) of $ZnFe_2O_4$Nanoparticles was calculated using the formula:

$$d_x = {}^{8M}/_{N_A a^3} \quad (3)$$

where d_x is the X-ray density, M is the relative molecular weight of the composition, N_A is Avogadro's number, and aaa is the lattice constant. The factor 8 reflects the presence of eight formula units per unit cell. The bulk density (dB) of the samples was determined using Archimedes' principle. The distances between magnetic ions, referred to as hopping lengths (L_A and L_B) at the tetrahedral (A) and octahedral (B) sites, were calculated using the appropriate relations [24, 25].

$$L_A = {}^{a\sqrt{3}}/_{4} \quad (4)$$

$$L_B = {}^{a\sqrt{2}}/_{4} \quad (5)$$

3.2 FTIRof $ZnFe_2O_4$Nanoparticles

The**Figure 3** presents the FTIR spectrum of $ZnFe_2O_4$ magnetic Nanoparticles (Nanoparticles) recorded at room temperature in the range of 350-4000 cm^{-1}. Spinel ferrites typically exhibit two characteristic absorption bands in the FTIR spectra within the 370-600 cm^{-1} region, attributed to metal-oxygen ($M-O$) stretching vibrations. In the $ZnFe_2O_4$ Nanoparticles, the higher wavenumber band at approx. 550 cm^{-1};($v1$) corresponds to $M-O$ stretching vibrations at the tetrahedral (A) site of the spinel lattice, where the metal-oxygen bond is shorter. Conversely, the lower wavenumber band close to400 $cm^{-1}(v2)$ is associated with $M-O$ stretching vibrations at the octahedral (B) site; characterized by a slightly longer metal-oxygen bond. These two distinct absorption bands serve as a characteristic "fingerprint" for spinel ferrites, providing valuable insights into their crystal structure and the bonding environment of metal ions within the lattice [27, 28]. The observed variations in bond lengths between the tetrahedral (A) and octahedral (B) sites significantly influence their vibrational frequencies. The shorter oxygen-iron bond length (1.89 Å) at the tetrahedral site results in stronger covalent bonding and consequently higher vibrational stretching frequencies compared to the longer oxygen-iron bond (1.99 Å) at the octahedral site, where weaker bonding leads to lower frequencies. This distinct vibrational behavior is a characteristic feature of spinel structures, arising from the specific

IJETIR
ISSN (Online) 2583-0554
International Journal of Emerging Technologies and Innovative Research (IJETIR)
Volume 3, Issue 1, February 2023
Impact Factor: 5.731

arrangement of cations within tetrahedral and octahedral voids. The presence of two distinct interstitial stretching modes, $v1$ and $v2$, in the FTIR spectrum directly confirms the spinel structure of $ZnFe_2O_4$Nanoparticles. These modes are characteristic of the spinel lattice, where the unique geometric arrangement of metal ions in tetrahedral and octahedral sites gives rise to these specific vibrational patterns. The clear differentiation between these vibrational modes in the FTIR spectrum further validates the material's spinel configuration. This phenomenon is not unique to $ZnFe_2O_4$ but is a hallmark of spinel ferrites, where subtle variations in bond lengths and coordination environments result in complex vibrational patterns. These seemingly small structural differences have significant implications for the material's overall properties, including its magnetic, electrical, and catalytic behaviors. The complexity observed in the FTIR spectrum reflects intricate molecular-level interactions within the material. This intricacy echoes Richard Feynman's observation that "the beauty of a flower may not be just in its color, but in the complexity it reveals. Similarly, in $ZnFe_2O_4$ and other ferrites, the true elegance lies in the intricate molecular interactions and the nuanced differences in bonding that underpin their unique physical properties [30].

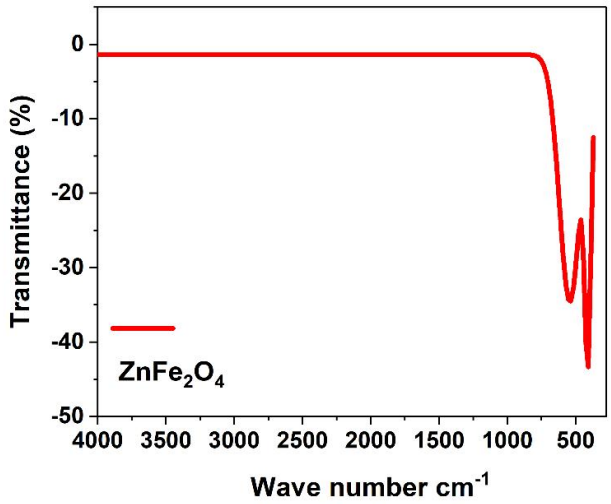

Figure 3 FTIR spectra of $ZnFe_2O_4$Nanoparticles

3.3 Magnetic property of $ZnFe_2O_4$Nanoparticles

The Magnetic properties of $ZnFe_2O_4$ samples, including saturation magnetization (Ms), remanent magnetization (Mr), coercivity (Hc), squareness ratio (Mr/Ms), and magneton number (nB), were determined using Pulse-Field Hysteresis Loop $(PFHL)$ measurements (**Figure 4**). The measured Ms and Mr suggest a disruption of exchange interactions at the nanoparticle surfaces, leading to surface-canted spins. The observed coercivity (Hc) is likely attributed to nanoscale size effects, influencing domain wall pinning and surface anisotropies. The squareness ratio (Mr/Ms) indicates a mixed multi-domain and single-domain magnetic behavior.In the inverted spinel structure of $ZnFe_2O_4$, Co^{2+} ions at the octahedral (B) sites contribute a magnetic moment, while the magnetic moments of Fe^{3+} ions at both tetrahedral (A) and octahedral (B) sites largely cancel each other due to antiferromagnetic coupling. The calculated magneton number (nB) per formula unit, suggests moderate $A-B$ site interaction, consistent with the typical magnetic behavior observed in spinel ferrites [31][33, 34].

$$n_B = \frac{[M_S \times M_W]}{558\ 5} \quad (6)$$

IJETIR
ISSN (Online) 2583-0554
International Journal of Emerging Technologies and Innovative Research (IJETIR)
Volume 3, Issue 1, February 2023
Impact Factor: 5.731

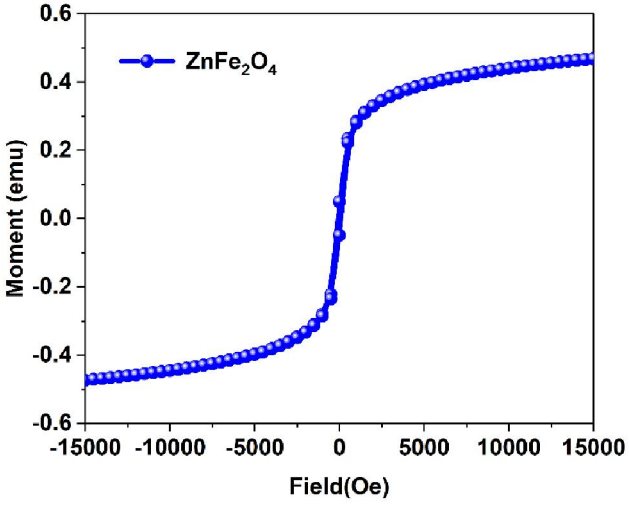

Figure 4 Hysteresis loop of $ZnFe_2O_4$ Nanoparticles

The surface anisotropy and spin canting, arising from reduced coordination and altered exchange interactions at the nanoparticle surface, contributed to a decrease in saturation magnetization and influenced the magnetic hysteresis behavior. These findings, consistent with theoretical predictions, underscore the significant impact of particle size, surface structural features, and synthesis conditions on the magnetic properties of $ZnFe_2O_4$Nanoparticles.

3.4 DC-resistivity of $ZnFe_2O_4$Nanoparticles

The Zinc ferrite exhibits high resistivity, exceeding $10^9\ \Omega \cdot cm$, classifying it as a highly resistive material. As shown in **Figure 5**, the DC resistivity of $ZnFe_2O_4$ Nanoparticles decreases with increasing temperature, characteristic of a conduction mechanism dominated by weak polaron hopping between Fe^{2+} and Fe^{3+} ions. This temperature dependence confirms the semiconducting nature of $ZnFe_2O_4$Nanoparticles. For characterization, the nanopowder was compressed into a 10 mm diameter, 2 mm thick pellet using a KBr press.

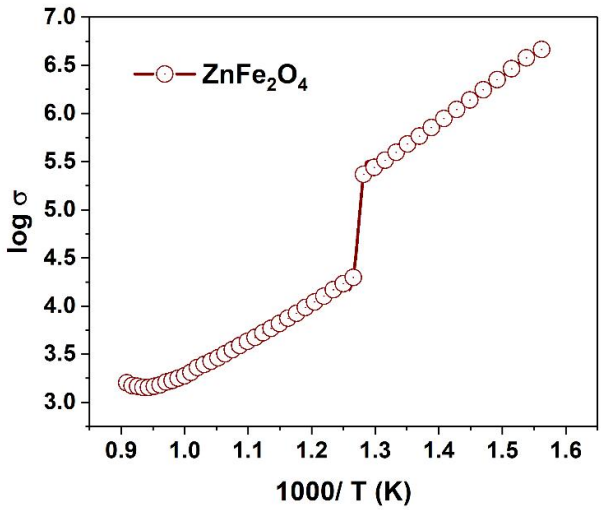

Figure 5 DC-electrical resistivity of $ZnFe_2O_4$Nanoparticles

DOI: 10.48175/IJETIR-1547

IJETIR
ISSN (Online) 2583-0554
International Journal of Emerging Technologies and Innovative Research (IJETIR)
Volume 3, Issue 1, February 2023
Impact Factor: 5.731

To ensure the reliable electrical contact, a thin layer of silver paste was applied to both sides of the pellet. The temperature-dependent DC resistivity was subsequently measured over the temperature range of 300-600 °C using a two-probe method. The DC resistivity of spinel ferrites is influenced by various factors, including the concentration of Fe^{2+} ions at octahedral (B) sites, grain size (G), sintering temperature, and porosity $(P\%)$. The electrical resistivity (ρ) was determined using the Arrhenius relation, which describes the temperature (T) dependence of DC resistivity [35];

$$\rho = \rho_0 \times \exp\left(\frac{\Delta E_a}{kT}\right) \quad (7)$$

The Arrhenius equation, $\rho = \rho_0\, exp(Ea/kT)$, describes the temperature dependence of DC resistivity, where ρ_0 is the temperature-independent resistivity, Ea is the activation energy, k is the Boltzmann constant, and T is the absolute temperature. The activation energy (Ea), determined to be in between $2.5 - 3.5\, eV$, governs the temperature-dependent mobility of charge carriers within the ferrite material. According to the Arrhenius relation, electrical resistivity decreases with increasing temperature, a characteristicbehavior of semiconductors. In $ZnFe_2O_4$Nanoparticles, this decrease in resistivity arises from an enhancement in charge carrier mobility at elevated temperatures. As temperature increases, more charge carriers acquire sufficient energy to overcome potential barriers, resulting in increased mobility and a corresponding decrease in resistivity;

$$\mu = 1/ne\rho \quad (8)$$

where μ is the mobility, e is the electronic charge, ρ is the resistivity, and n is the charge carrier concentration. The charge carrier concentration (n) can be calculated using the equation:

$$n = \frac{Na\rho P}{M_W} \quad (9)$$

where M_W is the molecular weight, NA is Avogadro's number, ρ is the sample density, and P represents the number of iron atoms in the oxide's chemical formula.

IV. CONCLUSIONS

TheThe sol-gel auto-combustion technique was effectively employed to synthesize $ZnFe_2O_4$ magnetic nanoparticles (Nanoparticles), with citric acid $(C_6H_8O_7)$ acting as the fuel. X-ray diffraction (XRD) analysis of the $ZnFe_2O_4$ Nanoparticles confirmed the formation of a cubic spinel structure, corresponding to the F_{d3m}-Oh_7 space group. The lattice constant (a) of the synthesized Nanoparticles was measured at $\sim 8.4 \pm 0.05$ Å. Peak broadening analysis using Debye-Scherrer's equation revealed an average crystallite size (t) in nanometer. The Fourier-transform infrared (FT-IR) spectra displayed two prominent metal-oxide bands at around 550 cm^{-1} (O-M Oct) and 400 cm^{-1} (O-M Td), which correspond to the metal-oxygen bonds at the octahedral and tetrahedral sites, respectively, within the $ZnFe_2O_4$ structure. These bands, which fall within the typical range of 370 to 600 cm^{-1} for spinel ferrites, confirmed the structural integrity of the synthesized material. Magnetic measurements showed a saturation magnetization (Ms); a remanent magnetization (Mr); and a magneton number (nB). DC electrical resistivity measurements, in agreement with the Arrhenius equation, confirmed the semiconducting nature of the $ZnFe_2O_4$Nanoparticles.

REFERENCES

[1] P.B. Kharat, S.B. Somvanshi, E.A. Dawi, A.M. Mopari, N.H. Bansod, Exploring the electrochemical performance of nickel-zinc ferrite nanoparticles for supercapacitor applications, Journal of Materials Science: Materials in Electronics, 35 (2024) 606.
[2] D.S. Mathew, R.-S. Juang, An overview of the structure and magnetism of spinel ferrite nanoparticles and their synthesis in microemulsions, Chemical engineering journal, 129 (2007) 51-65.
[3] H. Dawoud, S. Shaat, Magnetic properties of Zn substituted Cu ferrite, DOI (2006).
[4] Z. Ghasemian, D. Shahbazi-Gahrouei, S. Manouchehri, Cobalt zinc ferrite nanoparticles as a potential magnetic resonance imaging agent: An in vitro study, Avicenna journal of medical biotechnology, 7 (2015) 64.
[5] M. Qin, Q. Shuai, G. Wu, B. Zheng, Z. Wang, H. Wu, Zinc ferrite composite material with controllable morphology and its applications, Materials Science and Engineering: B, 224 (2017) 125-138.

[6] A. Singh, A. Singh, S. Singh, P. Tandon, B. Yadav, R. Yadav, Synthesis, characterization and performance of zinc ferrite nanorods for room temperature sensing applications, Journal of Alloys and Compounds, 618 (2015) 475-483.
[7] B. Anjaneyulu, Chinmay, V. Chauhan, S.A. Carabineiro, M. Afshari, Recent advances on zinc ferrite and its derivatives as the forerunner of the nanomaterials in catalytic applications, Journal of Inorganic and Organometallic Polymers and Materials, 34 (2024) 1887-1907.
[8] S. Latif, A. Liaqat, M. Imran, A. Javaid, N. Hussain, T. Jesionowski, M. Bilal, Development of zinc ferrite nanoparticles with enhanced photocatalytic performance for remediation of environmentally toxic pharmaceutical waste diclofenac sodium from wastewater, Environmental Research, 216 (2023) 114500.
[9] J. Garg, M.N. Chiu, S. Krishnan, R. Kumar, M. Rifah, P. Ahlawat, N.K. Jha, K.K. Kesari, J. Ruokolainen, P.K. Gupta, Emerging trends in zinc ferrite nanoparticles for biomedical and environmental applications, Applied Biochemistry and Biotechnology, 196 (2024) 1008-1043.
[10] A. Pradeep, P. Priyadharsini, G. Chandrasekaran, Structural, magnetic and electrical properties of nanocrystalline zinc ferrite, Journal of Alloys and Compounds, 509 (2011) 3917-3923.
[11] S. Zahi, M. Hashim, A. Daud, Synthesis, magnetic properties and microstructure of Ni–Zn ferrite by sol–gel technique, Journal of Magnetism and Magnetic Materials, 308 (2007) 177-182.
[12] U. Steinike, P. Druska, B. Wallis, D.C. Uecker, V. Sepelak, Formation and surface structure of Ti–Zn-double oxides and Zn ferrite, Chem Papers, 52 (1998) 147-151.
[13] B. Mishra, B. Munisha, J. Nanda, K. Sankaran, S. Suman, Hydrothermally Synthesized Magnesium doped Zinc Ferrite Nanoparticles: An extensive study on structural, optical, magnetic, and dielectric properties, Materials Chemistry and Physics, 292 (2022) 126791.